Suppressing Chest Radiograph Ribs for Improving Lung Nodule Visibility by using Circular Window Adaptive Median Outlier (CWAMO)

Dnyaneshwar Kanade[1], Jagdish Helonde[2]
Research Scholar, School of Engineering and Technology, Sandip University[1]
Professor, School of Engineering and Technology, Sandip University[2]

***Abstract*—Chest radiograph ribs obstruct lung nodules. To see the nodule under the chest radiograph ribs, remove or suppress them. The paper describes a circular median filter approach for finding outliers in chest radiographs. The method uses 147 Japanese Society of Radiological Technology x-ray pictures (JSRT). Pixels with intensities two standard deviations above the median are median outliers. Contrast-Limited Adaptive Histogram Equalization enhances nodule visibility (CLAHE). The method is tested on modest chest radiographs and compared to the Budapest University Bone Shadow Eliminated X-Ray Dataset methodology. The initial test uses 50 modest chest radiographs (Test 1). The proposed approach is applied after active shape modelling (ASM) lung segmentation. True positive nodules are seen on 89% of chest radiographs of various subtleties. Test-2 and Test-3 used 20 subtlety-level photos. In Test-2, the peak signal-to-noise ratio (PSNR), mean-to-standard deviation ratio (MSR), and universal image quality index (IQI) are evaluated for the full image and compared to the existing algorithm. For all three parameters, the suggested technique outperforms the algorithm. Test-3 computes nodule MSR and compares it to Budapest University's Bone Shadow Eliminated Dataset and original chest radiographs. The new algorithm improved nodule area contrast by 3.83% and 23.94% compared to the original chest radiograph. This approach improves chest radiograph nodule visualization.**

Keywords*—Lung cancer; chest radiograph; contrast limited adaptive histogram equalization; median outlier

I. Introduction

Imaging techniques such as radiography, magnetic resonance imaging (MRI), and computed tomography (CT) are all regularly utilized in the field of medical diagnosis for the purpose of locating lung cancer. Despite the fact that MRI and CT are more sensitive and accurate techniques, chest radiography is still the most recommended type of process for the initial diagnosis and detection of lung cancer due to the fact that it is a noninvasive form of operation, has a low radiation dosage, and is affordable. It is necessary to eliminate the shadow of the chest ribs from the chest radiograph before beginning the process of identifying candidate nodules from the chest radiograph. The chest rib shadows have been removed from the chest radiograph using a variety of methods that have been proposed in a number of studies. These methods also detect lung nodule-like components in the chest radiograph. This article discusses the elimination of chest rib shadows from chest radiographs using the median outlier technique and the detection of nodule-like parts using the thresholding technique. Both of these techniques are discussed in detail in Section III. Before the nodule was found, the images were improved using a technique called CLAHE. This allowed for a clearer view of the area. The lungs are segmented with ASM [1], [2], [3], [4]. The image database maintained by the JSRT [5] is utilized by the proposed approach (CWAMO). The proposed method is unsupervised and does not require either large dataset or training of it. The adaptive nature of the median outlier filter archives consistent results for differently illuminated chest radiographs. The proposed method is evaluated for its usefulness by calculating different measure such as PSNR, universal IQI and MSR for the entire image and nodule area and then compared them with the existing algorithm.

The paper can be structured in the following manner: In the Second II, several similar efforts on the removal of bone shadows from chest x-ray pictures are discussed. In the Section III of this research project, both the problem statement and the technique are discussed. Experimentation is performed in Section IV. Section V presents a comprehensive study of the currently used method as well as the proposed improvements, and Section VI brings the entire research to a close.

II. Related Work

The current state of the art incorporates a number of techniques for the suppression of ribs and the segmentation of lung nodules, all of which are based on standard chest radiography practices. The outcomes of the offered strategy are evaluated in light of the dataset called the "Bone Shadow Eliminated Image Dataset" [6] developed by Budapest University (BSE-BU). By appointing a slope to every point in the image, a one-of-a-kind process creates a model that ignores the information about its positioning. These slopes can be graphed using a slope field and are represented by a function that requires two inputs to operate. Three characteristics are sufficient to identify the ribcage, as indicated by research that was carried out on a range of tasks. The function was analyzed through the use of principal component analysis, which resulted in the generation of the function's final iteration, which was a two-variable, third-order rational function. Due to the fact that it spans chest bones, the nodule is difficult to identify with conventional chest radiography. Independent Component Analysis [7] is used in

the process, which suppresses the rear ribs and clavicles (ICA). By utilizing this method, the visibility of the nodule will be improved, and the strain on the automatic nodule recognition module will be decreased. Active appearance models and active shape models are integrated with a k-nearest neighbor classifier and a filter bank composed of different scales of Gaussian derivatives for the purpose of evaluating and contrasting various supervised segmentation algorithms. The techniques were tested using a database that was available to the general public and had 247 chest radiographs. In this database, all of the elements had been manually segmented by two human observers. The process of segmenting the clavicle is challenging regardless of the approach used [8]; dynamic shape models produce the greatest results, but the performance of humans is noticeably superior. Iterated contextual pixel classification (ICPC) [9] is an iterative, pixel-based, supervised, statistical classification procedure. The initial segmentation of the ribs acquired by pixel classification is updated by the ICPC, which does so by reclassifying each pixel by making use of both its original attributes and the knowledge regarding the class labels of neighboring pixels. The methodology is analyzed by using thirty radiographs taken from a database maintained by the JSRT. ICPC achieves a classification accuracy of 0.86 spl plus mn or 0.06 in an experiment using sixfold cross-validation, whereas the second human observer achieves an accuracy of 0.94 spl plus mn or 0.02 in the same experiment. In [10], x-rays is described. This system combines three different methods of doing so. The interior, border, and head of the clavicle are each classed in a separate category and divided into two stages, respectively. This is the data that is sent into the active shape model so that it can be segmented. In order to arrive at the desired end result, information regarding the shape obtained from the active shape model is combined with appearance data obtained from the inside of the clavicle, the border, the head, and dynamic programming. The method is evaluated against a wide variety of techniques that have been published in the past as well as against impartial human observers using a huge database. The approach that is advised produces a mean contour distance of 1.1 millimeters and an intersection over union distance of 0.86 millimeters when applied to 249 test photographs. a one-of-a-kind method that segments x-rays through the use of a dynamic programming strategy, so releasing them from the shadows that are cast by the rib cage and the clavicle [11]. When moving to a new place, the separated shadows will no longer be present. After being cleaned, the images are put through a hybrid lesion detector that uses data on gradient convergence, contrast, and intensity. The use of a support vector machine helps get rid of inaccurate findings. The method can eliminate 80% of bone shadows and 84% of them in the posterior region, despite having an average segmentation error of 1 millimeter. The frequency of false positives was reduced from 2,94 to 1 thanks to shadow reduction, which achieved a sensitivity of 63% for malignant tumors. The following is a rundown of the five primary stages involved in the suggested methods: After the lung has been segmented, the clavicle and ribs are located, their edges are determined, their profiles are computed, and suppression is carried out by making use of the projected profiles. The clavicle and the rib components are hidden from view in the image provided by the bone-suppression algorithm [12]. On a total of 491 photographs, the effectiveness of rib suppression was analyzed. It was found that 83.06% (or 6.59%) of the rib structures on a typical chest image were suppressed, which is approximately comparable to an average of one visible rib on a rib-suppressed image. This was discovered through the use of image analysis software. This conclusion was reached after comparing the rib areas recognized by the computer with the rib areas sketched by hand. Data mining and image processing are used to create a system for automatic rib recognition [13]. To begin, a number of template matching techniques and approaches based on graphs are employed to determine the position of the rib center line. After that, a support vector machine is utilized in order to model the way in which the ribs are positioned with respect to one another as well as to locate mistakes. In conclusion, decision trees are utilized in order to enhance the result of center line recognition. The JSRT dataset is used to conduct an analysis of the approach. The findings of rib recognition are greater than ninety-two percent for sensitivity and ninety-eight percent for specificity. A novel method expresses [14] that there is a different method for dividing up the ribs in chest radiography. Several applications of the Gaussian filter were required in order to get rid of the dataset's chaotic background. Detail images could be generated using the multi-scale wavelet decomposition, and then features extracted from the detail images using the Gaussian derivative. In order to properly categorize ribs, the support vector machine (SVM) rib model was developed. The convolutional neural filter (CNF) [15] for bone suppression is based on a convolutional neural network, which possesses excellent image processing capabilities and is frequently used in the field of medicine. [CNF] stands for "convolutional neural filter." The system that utilized CNF and consisted of six convolutional layers was successful in suppressing 89.2 percent of the bone. An intensive multitasking U-Net is offered as a solution to the problem of segmenting bones from a chest radiograph [16]. This solution is based on a sufficient dataset. A four-fold cross-validation is used to assess the performance of the proposed network on 88 chest radiograph pictures. The suggested technique for segmenting all bones results in average DSC values of 88.38%. These values are listed from highest to lowest. The proposed research produced lung digital x-rays, bone digital x-rays, and bone-free digital x-rays from 59 high-resolution CT images of the lung [17]. These DRs were utilized for the purpose of the suggested cascade convolutional neural network's internal evaluation as well as its training (CCNN). The authors propose an improved lung-simulated DR with varied bone intensity weightings by utilizing a 3-step image processing architecture. In addition to DR modeling and feature expansion, CT segmentation was also performed. Networks for bone identification and suppression are available through the CCNN. During the process of external validation, the trained CCNN was examined on a total of 30 chest radiographs. The clavicles and ribs have the ability to disguise even relatively minor abnormalities, which can lead to incorrect diagnoses. To reduce the number of radiological interpretation errors, particularly DL processes that are associated with tuberculosis identification, the purpose of this study [18] is to develop a

deep learning-based bone suppression model. This model will identify and remove these obstructing bony structures from the frontal CXRs (TB). Multiple bone suppression models, each with their own unique deep architectures, are trained, optimized, and finally evaluated at a number of different institutions using the combined loss function that was mentioned before. The theory was put to the test with the help of DeBoNet, which is a collection of models for convolutional neural networks [19] that inhibit frontal CXR bones. A specific collection of computed tomography images and their bone-suppressed analogues were used in the training and evaluation of U-Nets, Feature Pyramid Networks, and several other custom models. In terms of PSNR (36.797771.6210), MS-SSIM (0.98480.00), and other measures, DeBoNet surpassed the top three models that were used in its development. A novel approach generated a virtual dual energy (VDE) image with MTANN that suppressed ribs and clavicles to expose hidden nodules [20]. On chest radiographs, the ability of radiologists to detect pulmonary nodules was compared to the performance of bone suppression imaging using deep learning and bone subtraction imaging using a dual energy technique (CXRs) [21]. A completely automated system performs an analysis of digital posteroanterior (PA) chest radiographs [22]. This analysis begins with the segmentation of the lung field. Even the lungs that are normally neglected in conventional approaches are included in the segmented lung region because it includes the lungs that are concealed behind the heart, spine, and diaphragm. A projected nodule selection strategy is put into action once the partitioned region has been processed using a straightforward multiscale method in an effort to enhance the visibility of the nodules. To remove false positives, cost-sensitive support vector machines (SVMs) detect actual nodules. On two different feature-selected data sets, a number of Gaussian and polynomial SVM learning tests with variable parameter settings were carried out. The best SVM models have a false-positive rate of 1.5 per image when the sensitivity is set at 0.71. When the sensitivity is increased to 0.78 and 0.85, the rate increases to 2.5 and 4, respectively. The suggested approach generates seven or eight frames per second while maintaining the highest possible sensitivity (0.92–1.0). Using a Laplacian of Gaussian (LoG) filter as the basis for an approach to chest X-ray dot-like augmentation is discussed [23]. The directional texturing of lung nodules is improved when the X and Y axes are given the ability to have varied scale values. Image capture, image pre-processing, candidate nodule recognition, and feature extraction are the individual components that make up a computerized technique for recognizing nodules on chest radiographs [24]. The program is responsible for processing both SCLC and NSCLC pictures. In order to analyze the geometrical and textural properties of fifty photographs, twenty-five from each category were selected. Textural features were determined using GLCMs. Experiments involving the selection of image features provided novel results [25]. In order to get the best combination of traits, 210 different features were evaluated. Employing a procedure known as "forward stepwise selection," For each feature set, the area under the ROC curve served as the criterion for evaluation. It is suggested in [26] that images be pre-processed using a median filter. The thresholding method developed by Otsu is utilized in the segmentation process. The GLCM algorithm and various measurements of the physical dimensions are utilized throughout the process of feature extraction. ANNs are used to categorize the phases of disease. In this study, twenty-three wavelets from four different wavelet families—Daubechies, Haar, Biorthogonal, and Reverse Biorthogonal Spline—are compared in order to determine if lung nodules are benign or malignant [27]. In order for researchers to differentiate very small items from the background, they use three different sizes of regions of interest. For testing the suggested system, actual database pictures accompanied by tags are employed. Detecting lung nodules in chest radiographs is made possible by a computer system that uses multi-scale image processing [28]. This strategy accounts for the wide range of sizes that lung nodules can take, such as Active Shape Model lung field segmentation; quadratic classification with Lindeberg's multi-scale blob detector for nodule candidate detection; multi-scale edge focusing for blob segmentation; k-nearest neighbor classification; k-nearest neighbor classification. When looking at the comprehensive JSRT database, we find that allowing two false positives per image results in the detection of 50.6% of nodules. The percentage rises to 69.5% after the addition of 10 false positives. The classification of image thresholding techniques, the standardization of their formulas, and the comparison of their performances are all carried out [29]. The shape of the histogram, the grouping of the measurement space, the entropy of the data, the qualities of the objects, the spatial correlation, and the local gray-level surface data are all factors that differentiate the thresholding procedures. A comparison of forty different thresholding methods for nondestructive testing and document photos is shown here. Considering integrated performance indicators side by side We have developed thresholding methods that are more effective than nondestructive testing and document photography. Background may be removed with the help of the local mean and standard deviation, thanks to an innovative locally adaptive thresholding technique [30]. Integral sum image preparation calculates the local mean. A variance-based threshold selection criterion is developed by projecting the two-dimensional histograms of the original image and the local average image onto a one-dimensional space [31]. This results in the establishment of a variance-based threshold selection criterion. The suggested image thresholding strategy outperforms the Otsu, two-dimensional Otsu, and least class variance thresholding techniques, according to results obtained on bi-level and multi-level thresholding for artificial and real-world images. These results indicate that the proposed strategy is superior. The detailed study that provides a description of the finding of lung tumors on a chest graph [32] is presented. The approaches of watershed segmentation, thresholding, active contour, and differential operator, as well as expanding region [33], are compared. Two radiologists [34] used a retrospective investigation of a total of 100 patients, of whom 50% had lung nodules and the remaining 50% had no nodules, to confirm the chest CT findings. Using a computer-aided design (CAD) program, researchers compared four different methods for diagnosing lung nodules and masses. One hundred incidents were investigated in total. The mass algorithm outperformed the other three. A new hybrid deep

learning framework (CNN) was created by combining convolutional neural networks, visual geometry group-based neural networks (VGG), data augmentation, and spatial transformer networks (STN) [35]. The validation accuracy for the suggested technique is 73%, whereas the accuracy ratings for vanilla gray, vanilla RGB, hybrid CNN and VGG, and modified capsule networks are 67.8%, 69%, and 63.3%, respectively, for the complete dataset. An improved region growth (IRG) algorithm was used to segment the lung tumor in a way that was both more accurate and quicker than the traditional methods [36]. When applied to CT scans of four different patients, the overall strategy resulted in a 98% increase in segmentation accuracy when compared to the straightforward approach. The tumor was successfully contained by the multipoint growth-start combination. The technique improved tumor identification by a margin of less than 13% while also increasing compliance accuracy to an adequate level. A novel computer vision technology called understandable decision trees is used to predict the aggressiveness of lung cancer by employing decision trees [37]. This technique combines decision trees and deep learning. The deep learning component of this strategy was created with the use of a large set of pathological markers that are readily available to the public and are related to lung cancer. These techniques estimate chest X-ray biomarker scores utilizing two data sets tagged with malignancy. We found that fitting shallow decision trees to datasets that had been stratified based on the chance of cancer produced the best results. The most effective decision tree model has a specificity of 80%, a sensitivity of 86.7%, and a positive predictive value of 92.9%. Most of the proposed techniques are supervised in nature and need large dataset. These techniques also require training the model which takes lot of time. On the other hand, the non-supervised techniques proposed by other researchers assume equal illumination of all the images which is not the case in reality.

III. Proposed Method

A. Assumptions

Prior to using the proposed method for suppressing the chest radiograph ribs for improving nodule visibility and detecting nodule-like areas, the following assumptions are made:

1) The JSRT digital x-ray images [6] with bone shadow are the ones that were used for the dataset for the suggested approach. The dataset is made up of 154 traditional chest radiographs that show a lung nodule and 93 radiographs that do not show a lung lesion.

2) In the JSRT dataset, each chest radiograph with a lung nodule has only one nodule.

3) The study makes use of images ranging from a subtlety level of 5 (the nodule is extremely evident) to a subtlety level of 2 (the nodule is very subtle). The proposed method doesn't use images with a subtlety level of 1, which is sometimes called "very subtle," because it's very hard to pull nodules out of those images because they have low contrast, are small, or overlap with normal structure.

4) The circular median filter used has a radius of 50 pixels, and the threshold used is two standard deviations.

5) The block size of CLAHE [1] is 127, and the number of histogram bins is 256.

6) The maximum slop of CLAHE is 10.

7) For comparing the proposed method results, the JSRT bone shadow-eliminated images dataset by Budapest University (BSE-BU) [7] is used.

B. Algorithm

The proposed method is divided into five steps, namely: (1) Preprocessing of the image (2) Chest radiograph suppression (3) Contrast enhancement using CLAHE (4) Lung segmentation using ASM (5) Candidate nodule detection using Bernsen local contrast thresholding with a circular window (CWLCT) (Fig. 1).

1) Preprocessing of chest radiograph: In the preprocessing phase, the original chest radiograph pictures are boosted for contrast and then down sampled to a resolution of 1024 by 1024 pixels, which is a reduction from their original size of 2048 by 2048 pixels, before being used to suppress rib shades.

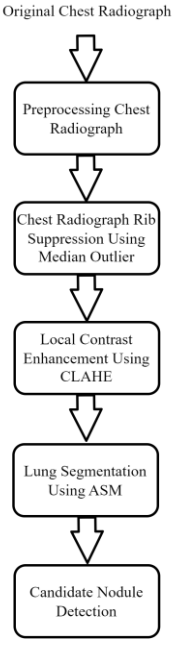

Fig. 1. System flow chart.

2) Chest radiograph rib suppression using median outlier: A circular median filter is applied to the chest radiograph in order to reduce the visibility of the ribs' shadows. The size of the image and the maximum height of a rib on the chest radiograph are used to establish the value for the radius of the circular median filter. The circular window was centered at the pixel *f(x,y)* to calculate the median of the pixel intensities of the image region under the circular window. By using the standard deviation as the threshold value, the pixel intensity at *f(x,y)* will be replaced with the median value ***m*** if it is brighter than the median by the

threshold value t; otherwise, it will be kept at its original value.

$$I_1(x,y) = \begin{cases} m \; if \; I(x,y) > m + t \\ I(x,y) \; otherwise \end{cases} \quad (1)$$

Where *I(x,y)* is the original gray level intensity at pixel *f(x,y)* and $I_1(x,y)$ is modified gray level intensity at pixel *f(x,y).*

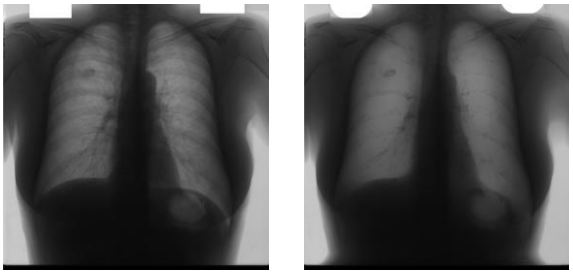

(a) (b)

Fig. 2. Rib suppression. (a) Original chest radiograph. (b) Rib suppressed chest radiograph.

Fig. 2(a) shows original chest radiograph while Fig. 2(b) shows ribs suppressed image using proposed AMO method.

3) Local contrast enhancement by CLAHE: Due to the concentration of the histogram in regions with nearly constant contrast, standard AHE has a tendency to overamplify the contrast in these areas. AHE may thus lead to noise amplification in regions with near-constant noise. In order to lessen the issue of noise amplification, contrast amplification is restricted in adaptive histogram equalization (CLAHE).

The magnitude of the contrast amplification in CLAHE close to a particular pixel value is determined by the slope of the transformation function. This is proportional to the value of the histogram at that pixel value as well as the slope of the cumulative distribution function (CDF) for the surrounding area. Before computing the CDF, CLAHE performs a clipping operation on the histogram at a value that has been previously determined in order to reduce amplification. Because of this, the slope of the transformation function is restricted due to the constraints placed on it. The so-called clip limit, also known as the value at which the histogram is clipped, is established based on the normalization of the histogram and, as a direct consequence of this, the size of the neighborhood region. Fig. 3(c) shows an enhanced image using CLAHE.

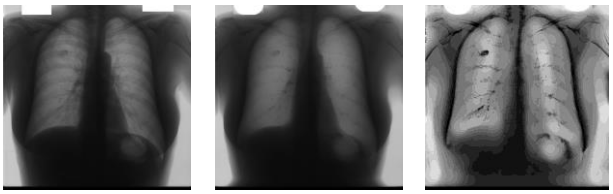

(a) (b) (c)

Fig. 3. Contrast enhancement using CLAHE (a) Original chest radiograph. (b) Rib suppressed chest radiograph (c) Contrast enhanced image.

4) Lung segmentation: An active shape model is used for extracting lung areas from the chest radiograph. One of the most reliable methods for picture segmentation is ASM. The active shape model is a parameterized contour model. The parameters are obtained using principal component analysis (PCA) and the statistics of numerous sets of points collected from various contours of comparable images. In ASM, the object's boundary is established by n points. These points produce the descriptor vector, which is generated as

$$x = (x_1, y_1, x_2, y_2, \ldots\ldots x_n, y_n)^T \quad (2)$$

where x_i and y_i are the i-th point on the contour's *x* and *y* coordinates respectively. The principal component analysis-calculated s training vectors have a mean shape of

$$\bar{x} = \frac{1}{s}\sum_{i=1}^{s} x_i \quad (3)$$

There will be a covariance matrix, defined as

$$S = \frac{1}{1-s}\sum_{i=1}^{s}(x_i - \bar{x})(x_i - \bar{x})^T \quad (4)$$

The covariance matrix's first t biggest Eigen values are picked. Due to the fact that only the eigenvalues with the greatest significance are taken into account, the number of parameters is drastically reduced and ultimately falls below n. The appropriate eigenvectors are all present in the matrix. The model's inputs are calculated as follows:

$$b = \Phi(x - \bar{x}) \quad (5)$$

From this, the approximate form is determined as follows.

$$x \approx \bar{x} + \Phi b) \quad (6)$$

(a) (b) (c)

Fig. 4. Lung segmentation. (a) Original chest radiograph. (b) ASM lung mask. (c) Lungs part of chest radiograph.

The appropriate b vector is found for a given contour when all of its components fall inside the range ±m√λi, with the right constant m. Starting with the mean shape, the parametric description of an object's contour is looked up. Until convergence or a preset number of iterations are reached, two alternate steps are used. Each contour point perpendicular to the contour is moved in the first step of the procedure. After numerous iterations of position testing on both sides of the contour, the ideal position is identified. Picture resolution is used in the training model to determine where an intensity gradient profile should be placed at each contour node. Finally, the ideal replacement location for the contour point is determined using the Mahalanobis distance. Then, all of the contour points are modified in order to fit a model to the new point set. The ideal b parameter is searched using (6). As the image's spatial resolution increases, the entire procedure is repeated numerous times. The proposed method used 100 chest radiographs from the JSRT dataset to train the model. The original chest radiograph is shown in Fig. 4(a). Fig. 4(b) displays the segmented lung mask that was produced using ASM. By using this mask on the original X-ray image, as seen in Fig. 4(c), the lungs are segmented.

5) Candidate nodule detection: The proposed method uses Bernsen local contrast thresholding [38] with a circular window with diameter w for image binarization instead of a square window while calculating local contrast, as shown in Fig. 5. For pixel P centered at i and j, a square window of size w x w takes 22% more neighboring pixels into account than the circular window having diameter w. The circular window used in the proposed method for image binarization plays an important role while calculating the local contrast for the boundary pixels of the true positive nodule. In the post-processing stage, morphological operations are used to remove unwanted regions. A significant reduction in false positive nodules is obtained by using prior knowledge of the true positive nodule. Based on the circularity index of the candidate nodules final candidate nodule segmented image is obtained as shown in Fig. 6(b) the white nodule is true positive while gray is false positive.

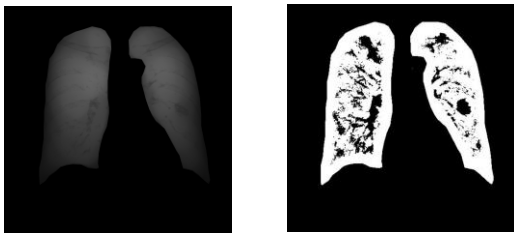

(a) (b)

Fig. 5. Local contrast thresholding. (a) Rib suppressed chest radiograph. (b) Binarization using local contrast thresholding.

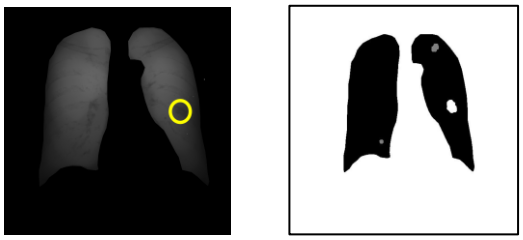

(a) (b)

Fig. 6. Post processing. (a) Original chest radiograph with annotation. (b) Candidate nodules (White is True Positive).

IV. Experimentation and Results

1) Test-1: 50 images with subtlety level 5 to 2 are used for experimentation. After preprocessing and lung segmentation using ASM, circular window local contrast thresholding technique applied for binarization. It is observed that the 90 % of the true positive nodules extracted are part of candidate nodules. The average rate of false positive nodules per image is 3.5 fp/image. Fig. 7 shows the results of candidate nodules extraction using local contrast thresholding with circular window for the images with subtlety level 5 to 2.

2) Test-2: Test-2 deals with the image quality measures of the proposed rib suppression algorithm by comparing it's results with the (Budapest University Bone Eliminated JSRT dataset) existing algorithm [7]. The second test, known as Test-2, evaluates entire image quality. In Test-2, we make use of the sample original images; images from the Budapest University Bone Eliminated JSRT dataset, as well as images obtained utilizing the proposed approaches. The quality of the images was evaluated in this study with the use of a number of different criteria. The criteria that will be used for the evaluation are 1) Peak Signal to Noise Ratio (PSNR), 2) Mean to Standard Deviation Ratio (MSR), and 3) Universal Quality Index (IQI).

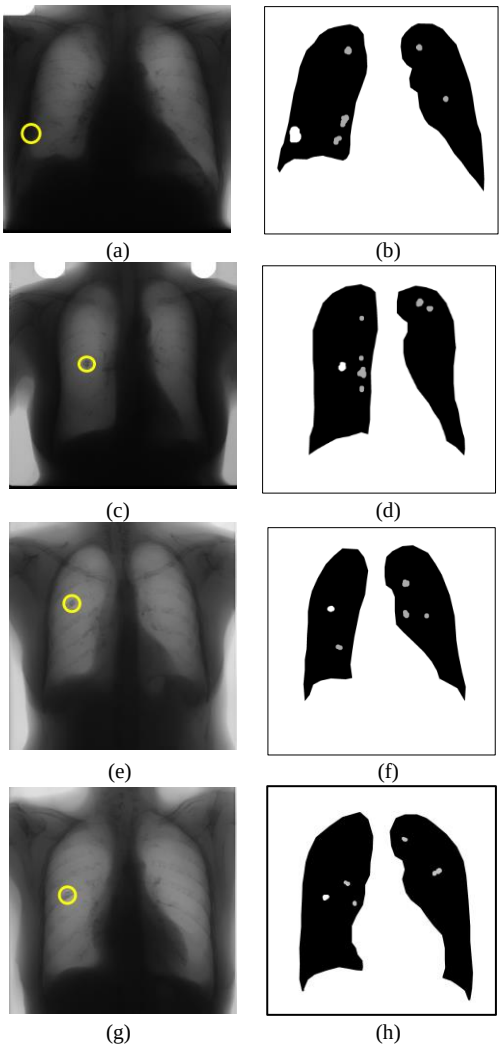

(a) (b) (c) (d) (e) (f) (g) (h)

Fig. 7. Some of the results obtained -Rib suppressed using proposed method Images with subtlety levels 5,4,3 & 2 sequentially (Left Column-(a), (c), (e), (g)), results of candidate nodule segmentation (White-True positive nodules) using local contrast thresholding and circular window (Right column-(b), (d), (f), (h)).

For image level analysis all above three measures are used while for nodule area analysis only MSR is used.

a) Test 2.1 Peak signal-to-noise ratio: Peak signal-to-noise ratio (PSNR) is expressed in decibels (dB) (decibels). PSNR is defined as

$$PSNR = 20log_{10}\left(\frac{MAX_I}{\sqrt{MSE}}\right) \quad (7)$$

where MAX_I is the highest value a pixel can have within an image, and MSE is determined by:

$$MSE = \frac{1}{ij}\sum_{m=0}^{i-1}\sum_{n=0}^{j-1} \| I(m,n) - K(m,n) \|^2 \quad (8)$$

Where I is original JSRT database image and K is either Budapest Bone Shadow Eliminated Image or Rib suppressed image using proposed method. Table I shows comparison of PSNR of Budapest University Images and result Images of the proposed method while Fig. 8 shows it graphically.

TABLE I. PEAK SIGNAL TO NOISE RATIO (PSNR)

Image	PSNR Existing Algorithm*	PSNR Proposed Method
JPCLN002.jpg	7.375601102	7.678650215
JPCLN003.jpg	12.11304948	12.47926008
JPCLN005.jpg	12.56962625	12.98963757
JPCLN006.jpg	9.227926597	9.618855472
JPCLN029.jpg	11.94079299	12.33675425
JPCLN034.jpg	12.1818185	13.05766792
JPCLN035.jpg	9.780592944	10.31366197
JPCLN041.jpg	11.88327603	12.30280025
JPCLN051.jpg	9.417197293	9.792465158
JPCLN052.jpg	9.856187759	10.17043184
JPCLN053.jpg	10.80607195	11.4255127
JPCLN058.jpg	11.31527493	11.97189975
JPCLN103.jpg	8.502726484	9.266778262
JPCLN104.jpg	11.25931517	11.85082129
JPCLN114.jpg	8.586153337	8.942296706
JPCLN116.jpg	9.779299456	10.15226717

*Existing Algorithm-Bone Shadow Eliminated X-Ray image dataset by Budapest University

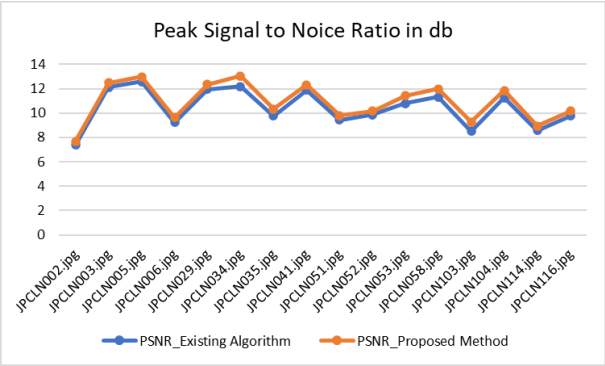

Fig. 8. PSNR using budapest bone shadow eliminated images dataset (existing algorithm) and proposed method.

b) Test 2.2 Mean to standard deviation ratio of Image: After calculating the mean and standard deviation of the entire image, it is simple to calculate the mean-to-standard deviation ratio (MSR). MSR stands for mean to standard deviation ratio. It would be better if MSR increased. Table II shows comparison of MSR of JSRT original images, Budapest University Images and result Images of the proposed method while Fig. 9 shows it graphically.

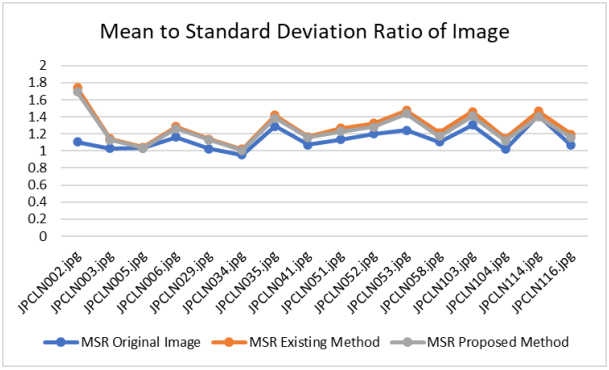

Fig. 9. Comparison between Image MSR of original image, MSR of budapest bone shadow eliminated images dataset and MSR of proposed method.

TABLE II. MEAN TO STANDARD DEVIATION RATIO (MSR)

Image	Original Image	Existing Method*	Proposed Method
JPCLN002.jpg	1.105865187	1.73929548	1.69239946
JPCLN003.jpg	1.029805377	1.143003543	1.130802017
JPCLN005.jpg	1.034735271	1.042355194	1.036175145
JPCLN006.jpg	1.163311881	1.285875138	1.260937779
JPCLN029.jpg	1.026111427	1.139242171	1.128066868
JPCLN034.jpg	0.953965214	1.021915224	1.00740993
JPCLN035.jpg	1.28773162	1.418071626	1.386284991
JPCLN041.jpg	1.072865683	1.166067981	1.158654616
JPCLN051.jpg	1.13379032	1.264658084	1.22893067
JPCLN052.jpg	1.19827801	1.32425825	1.278240793
JPCLN053.jpg	1.242163322	1.475137804	1.436426986
JPCLN058.jpg	1.106253489	1.215176321	1.17012551
JPCLN103.jpg	1.30222145	1.459562579	1.409503867
JPCLN104.jpg	1.02032688	1.146969601	1.117281164
JPCLN114.jpg	1.413209042	1.465449364	1.396894366
JPCLN116.jpg	1.066277074	1.195911959	1.158528356

*Existing Algorithm-Bone Shadow Eliminated X-Ray image dataset by Budapest University

c) Test 2.3 Universal image quality index: The image similarity across Rib suppression using existing algorithm and proposed method can be measured.

Let $I = \{i_n | n = 1, 2, ..., N\}$ and $J = \{j_n | n = 1, 2, ..., N\}$ be the original and Rib suppressed image signals, respectively. Universal image quality index (UQI) [39] is defined as

$$Q = \frac{4\sigma_{ij}\bar{i}\,\bar{j}}{\left(\sigma_i^2+\sigma_j^2\right)[(\bar{i})^2+(\bar{j})^2]} \quad (9)$$

The average pixel intensity of the original image is denoted by $\bar{i}$ and $\bar{j}$ indicates average pixel intensities of the Rib suppressed images. The minimum value of Q is 0 and maximum value of Q is 1, where the value 1 is considered to be the best value. It is only possible if and only if $i_n = j_n$ for all $n = 1, 2, ..., N$.

Table III shows comparison of MSR of JSRT original images, Budapest University Images and result Images of the proposed method while Fig. 10 shows it graphically.

TABLE III. UNIVERSAL QUALITY INDEX (IQI)

Image	Existing Algorithm	Proposed Method
JPCLN002.jpg	0.766393412	0.786052698
JPCLN003.jpg	0.559502642	0.6154612
JPCLN005.jpg	0.5484891	0.62938914
JPCLN006.jpg	0.888165856	0.918416024
JPCLN029.jpg	0.550828852	0.59797016
JPCLN034.jpg	0.951746077	0.982698381
JPCLN035.jpg	0.64269835	0.664188397
JPCLN041.jpg	0.518551926	0.552074836
JPCLN051.jpg	0.530794333	0.55762417
JPCLN052.jpg	0.888784908	0.921368415
JPCLN053.jpg	0.87828747	0.899798241
JPCLN058.jpg	0.875172812	0.918980863
JPCLN103.jpg	0.838295369	0.843335781
JPCLN104.jpg	0.707448061	0.734453776
JPCLN114.jpg	0.867494523	0.905721354
JPCLN116.jpg	0.640720912	0.691021895

*Existing Algorithm-Bone Shadow Eliminated X-Ray image dataset by Budapest University

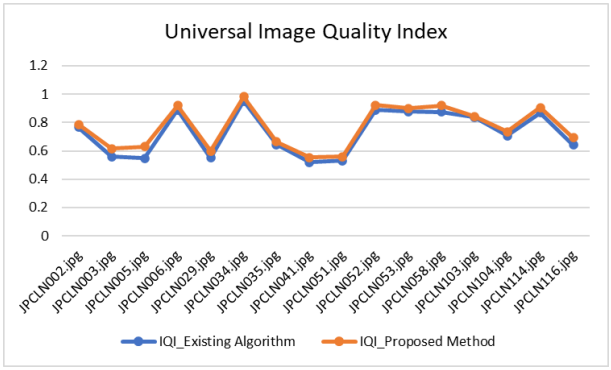

Fig. 10. Universal image quality using budapest bone shadow eliminated images dataset and proposed method.

3) Test-3

a) Test 3.1 Mean to standard deviation ratio of nodule area: In Test-3, the MSR is calculated for the nodule region, which takes into account its surroundings as well. The MSR of the nodule area calculated using the suggested method is compared to the MSR of the nodule area calculated using JSRT's original dataset and Budapest University's Bone Shadow Eliminated Image dataset. The Fig. 11(c) shows the sample result of the nodule area after suppressing ribs shadow from the chest radiograph using proposed method.

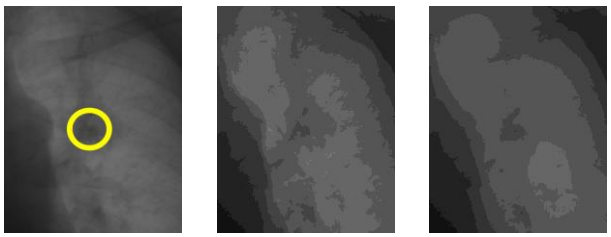

(a) (b) (c)

Fig. 11. Cropped nodule area (a) Nodule area in the original chest radiograph, (b) Nodule area in budapest bone shadow eliminated images dataset (c) Nodule area in the proposed method.

V. RESULT ANALYSIS

To evaluate the performance of the proposed method, a total of three tests are conducted. In Test-1, fifty images from the JSRT dataset with subtlety levels ranging from 5 to 2 are utilized. After preprocessing, the lungs are segmented using ASM. The ribs are removed using the proposed method (CWAMO), and finally, candidate nodules are extracted using circular window-based local contrast thresholding (CWLCT). From the results, it is observed that in 89% of the chest radiographs, true positive nodules are detected accurately. Test-2 was conducted to evaluate the performance of the proposed method at the image level. In this test, three measures were used for evaluation, namely PSNR, MSR, and IQI. Table I and Table III show the PSNR and IQI comparison between the existing algorithm and the proposed method. Fig. 8 and 10 depict it graphically. Table II shows the MSR comparison between the original image (with rib shadows), the bone shadow-eliminated image by Budapest University, and the proposed method (CWAMO). Fig. 9 shows the above comparison graphically. Four sample images ranging in subtlety from 5 to 2 were used for each of the measures.

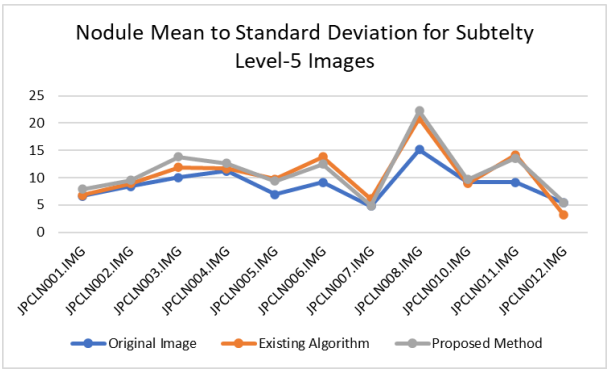

Fig. 12. Comparison between nodule MSR of original image, MSR of budapest bone shadow eliminated images dataset and MSR of proposed method for subtlety level-5.

As shown in Fig. 12, 13, 14, and 15, Test-3 employs ten sample images from each subtlety level (Level 5 to Level 2). It is observed that for all the above subtlety-level images, the proposed method performs equally with the existing algorithm.

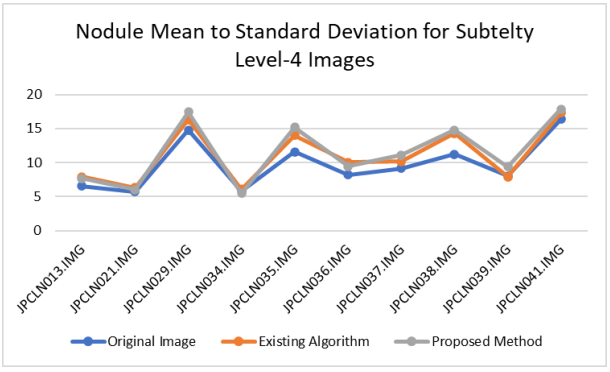

Fig. 13. Comparison between nodule MSR of original image, MSR of budapest bone shadow eliminated images dataset and MSR of proposed method for subtlety level-4.

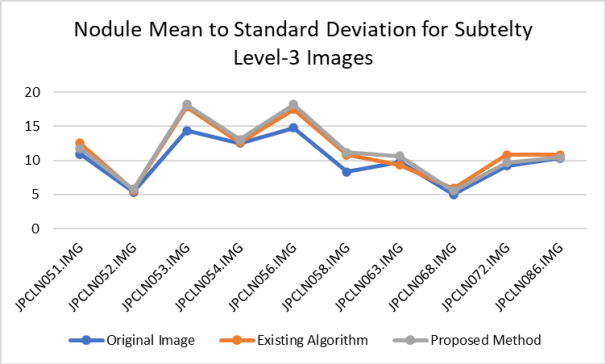

Fig. 14. Comparison between nodule MSR of original image, MSR of budapest bone shadow eliminated images dataset and MSR of proposed method for subtlety level-3.

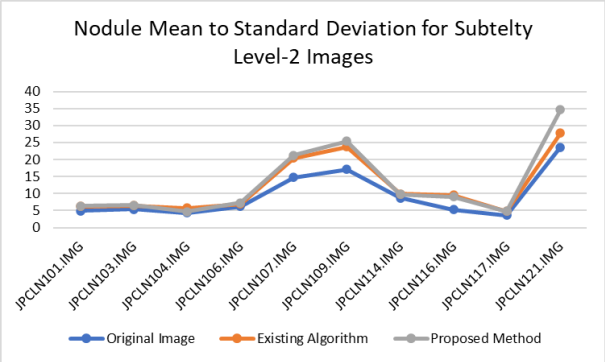

Fig. 15. Comparison between nodule MSR of original image, MSR of budapest bone shadow eliminated images dataset and MSR of proposed method for subtlety level-2.

For all three image quality measures, the proposed method performs over and above the existing algorithm. The ROI for evaluation in Test-3 was the nodule area, including its surroundings.

VI. Conclusion

The proposed work of bone suppression on chest radiographs using proposed method (CWAMO) achieves the goal of enhancing the accuracy of nodule detection in the chest radiographs. The first experimental setting, known as Test-1, uses chest radiograph images with modest levels 5 to 2 to detect actual positive nodules with an accuracy of 89%. This results in a significant reduction in the number of false positive nodules found in each image. During Test-2, the peak signal-to-noise ratio (PSNR), the mean-to-standard deviation ratio (MSR), and the universal image quality index (IQI) are analyzed for the entire image and compared with existing algorithm. The suggested technique performs better than the existing algorithm across all three parameters. Test-3 calculates the nodule MSR and then compares it to the Bone Shadow Eliminated Dataset created by Budapest University as well as the original chest radiographs. When compared to the existing bone shadow eliminated dataset, the new algorithm achieved an improvement in nodule area contrast of 3.83% and 23.94% shadow. This strategy results in an improvement in the visibility of nodules on chest radiographs. In conclusion, the utilization of CWAMO not only eliminates the shadow that is cast by the ribs on the chest radiograph, but it also assists in the localization of the nodules that are obscured by the shadows cast by the bones on the chest radiograph.

References

[1] T. Cootes, “An Introduction to Active Shape Models,” in Image Processing and Analysis, Ed.R.Baldock and J.Graham, Eds. Oxford University Press, 2000, pp. 223–248.

[2] T. F. Cootes, A. Hill, C. J. Taylor, and J. Hastam, “Use of active shape models for locating structures in medical images,” Image Vis Comput, vol. 12, no. 6, pp. 355–365, 1994.

[3] J.-Shyang. Pan, B.-Long. Guo, A. Abraham, Xi’an dian zi ke ji da xue., Guo li Gaoxiong ying yong ke ji da xue., and IEEE Computer Society., “Lung segmentation for chest radiograph by using adaptive active shape models,” in 2009 Fifth International Conference on Information Assurance and Security, 2009, pp. 383–386. Accessed: Feb. 20, 2023. [Online]. Available: 10.1109/IAS.2009.353.

[4] B. Van Ginneken, A. F. Frangi, J. J. Staal, B. M. Ter Haar Romeny, and M. A. Viergever, “Active shape model segmentation with optimal features,” IEEE Trans Med Imaging, vol. 21, no. 8, pp. 924–933, Aug. 2002, doi: 10.1109/TMI.2002.803121.

[5] S. Junji et al., “A Development of a Digital Image Database for Chest Radiographs With and Without a Lung Nodule: Receiver Operating Characteristic Analysis of Radiologists’ Detection of Pulmonary Nodules,” American journal of roentgenology, vol. 174, pp. 71–74, 2000, [Online]. Available: www.macnet.or.jp/jsrt2/.

[6] S. Juhász, Á. Horváth, L. Nikházy, and G. Horváth, “Segmentation of Anatomical Structures on Chest Radiographs,” in Medicon 2010, IFMBE Proceedings 29, 2010, pp. 359–362. [Online]. Available: www.springerlink.com.

[7] A. Bilal, R. Tahir, A. ,U. , K. Mohammad, R. Abdur, and A. Saghir, “Rib Suppression in chest radiographs using ICA,” Information Technology Journal, vol. 6, no. 7, pp. 1085–1089, 2007.

[8] B. van Ginneken, M. B. Stegmann, and M. Loog, “Segmentation of anatomical structures in chest radiographs using supervised methods: A comparative study on a public database,” Med Image Anal, vol. 10, no. 1, pp. 19–40, Feb. 2006, doi: 10.1016/j.media.2005.02.002.

[9] M. Loog and B. Van Ginneken, “Segmentation of the posterior ribs in chest radiographs using iterated contextual pixel classification,” IEEE Trans Med Imaging, vol. 25, no. 5, pp. 602–611, May 2006, doi: 10.1109/TMI.2006.872747.

[10] L. Hogeweg, C. I. Sánchez, P. A. de Jong, P. Maduskar, and B. van Ginneken, “Clavicle segmentation in chest radiographs,” Med Image Anal, vol. 16, no. 8, pp. 1490–1502, 2012, doi: 10.1016/j.media.2012.06.009.

[11] Á. Horváth, G. Orbán, Á. Horváth, and G. Horváth, “An X-ray CAD system with ribcage suppression for improved detection of lung lesions,” Periodica Polytechnica Electrical Engineering and Computer Science, vol. 57, no. 1, pp. 19–33, 2013, doi: 10.3311/PPee.2079.

[12] Z. Huo et al., “Bone suppression technique for chest radiographs,” in Medical Imaging 2014: Image Perception, Observer Performance, and Technology Assessment, Mar. 2014, vol. 9037. doi: 10.1117/12.2043754.

[13] X. Li, S. Luo, and Q. Hu, “An Automatic Rib Segmentation Method on X-Ray Radiographs,” in International Conference on Multimedia Modeling, 2015, vol. 8935, pp. 128–139.

[14] W. Haiping and Z. Guodong, “Rib Segmentation in Chest Radiographs by Support Vector Machine,” in International Conference on Education, Management, Computer and Society (EMCS 2016), 2016.

[15] N. Matsubara, A. Teramoto, K. Saito, and H. Fujita, “Bone suppression for chest X-ray image using a convolutional neural filter,” Australas Phys Eng Sci Med, vol. 43, 2019, doi: 10.1007/s13246-019-00822-w.

[16] W. Wang et al., “MDU-Net: A Convolutional Network for Clavicle and Rib Segmentation from a Chest Radiograph,” J Healthc Eng, vol. 2020, 2020, doi: 10.1155/2020/2785464.

[17] G. Ren et al., “Deep learning-based bone suppression in chest radiographs using CT-derived features: A feasibility study,” Quant Imaging Med Surg, vol. 11, no. 12, pp. 4807–4819, Dec. 2021, doi: 10.21037/qims-20-1230.

[18] S. Rajaraman, G. Zamzmi, L. Folio, P. Alderson, and S. Antani, "Chest X-Ray Bone Suppression for Improving Classification of Tuberculosis-Consistent Findings," Diagnostics (Basel), vol. 11, no. 5, 2021, doi: 10.3390/diagnostics11050840.

[19] S. Rajaraman, G. Cohen, L. Spear, L. Folio, and S. Antani, "DeBoNet: A deep bone suppression model ensemble to improve disease detection in chest radiographs," PLoS One, vol. 17, no. 3, Mar. 2022, doi: 10.1371/journal.pone.0265691.

[20] S. Chen and K. Suzuki, "Computerized detection of lung nodules by means of 'virtual dual-energy' radiography," IEEE Trans Biomed Eng, vol. 60, no. 2, pp. 369–378, 2013, doi: 10.1109/TBME.2012.2226583.

[21] K. Bae, D. Y. Oh, I. D. Yun, and K. N. Jeon, "Bone Suppression on Chest Radiographs for Pulmonary Nodule Detection: Comparison between a Generative Adversarial Network and Dual-Energy Subtraction," Korean J Radiol, vol. 23, no. 1, pp. 139–149, Feb. 2022, doi: 10.3348/kjr.2021.0146.

[22] P. Campadelli, E. Casiraghi, and D. Artioli, "A fully automated method for lung nodule detection from postero-anterior chest radiographs," IEEE Trans Med Imaging, vol. 25, no. 12, pp. 1588–1603, Dec. 2006, doi: 10.1109/TMI.2006.884198.

[23] **00**Z. Shi, J. Bai, K. Suzuki, L. He, Q. Yao, and T. Nakamura, "A Method for Enhancing Dot-like Regions in Chest X-rays Based on Directional Scale LoG Filter," Journal of Information & Computational Science, vol. 7, no. 8, pp. 1689–1696, 2010, [Online]. Available: http://www.joics.com.

[24] S. A. Patil and V. R. Udupi, "Chest X-ray features extraction for lung cancer classification," J Sci Ind Res (India), vol. 69, pp. 271–277, 2010.

[25] J. Wei, Y. Hagihara, A. Shimizu, and H. Kobatake, "Optimal image feature set for detecting lung nodules on chest X-ray images," Computer Assisted Radiology and Surgery, Springer, 2002, [Online]. Available: https://doi.org/10.1007/978-3-642-56168-9_118.

[26] K. Mya, M. Tun, and A. Soe Khaing, "Feature Extraction and Classification of Lung Cancer Nodule using Image Processing Techniques," International Journal of Engineering Research & Technology , vol. 3, no. 3, 2014, [Online]. Available: www.ijert.org.

[27] A. M. Al Gindi, E. A. Rashed, and M.-S. M. Mostafa, "Development and Evaluation of a Computer-Aided Diagnostic Algorithm for Lung Nodule Characterization and Classification in Chest Radiographs using Multiscale Wavelet Transform," Journal of American Science, vol. 10, no. 2, pp. 1545–1003, 2014, [Online]. Available: http://www.jofamericanscience.orghttp://www.jofamericanscience.org.14.

[28] A. M. R. Schilham, B. Van Ginneken, and M. Loog, "Multi-scale Nodule Detection in Chest Radiographs," in International Conference on Medical Image Computing and Computer-Assisted Intervention, 2003, pp. 602–609. [Online]. Available: http://www.isi.uu.nl.

[29] S. Mehmet and S. Bulent, "Survey over image thresholding techniques and quantitative performance evaluation," J Electron Imaging, vol. 13, no. 1, pp. 146–165, Jan. 2004, doi: 10.1117/1.1631316.

[30] T. R. Singh, S. Roy, O. I. Singh, T. Sinam, and K. M. Singh, "A New Local Adaptive Thresholding Technique in Binarization," International Journal of Computer Science Issues, vol. 8, no. 6, Nov. 2011, [Online]. Available: www.IJCSI.org.

[31] F. Nie, Y. Wang, M. Pan, G. Peng, and P. Zhang, "Two-dimensional extension of variance-based thresholding for image segmentation," Multidimens Syst Signal Process, vol. 24, no. 3, pp. 485–501, Sep. 2013, doi: 10.1007/s11045-012-0174-7.

[32] S. K. Chaya Devi and T. Satya Savithri, "Review: On segmentation of nodules from posterior and anterior chest radiographs," Int J Biomed Imaging, vol. 2018, pp. 1–11, Oct. 2018, doi: 10.1155/2018/9752638.

[33] L. Zheng and Y. Lei, "A Review of Image Segmentation Methods for Lung Nodule Detection Based on Computed Tomography Images," in MATEC Web of Conferences, Nov. 2018, vol. 232. doi: 10.1051/matecconf/201823202001.

[34] C. H. Liang, Y. C. Liu, M. T. Wu, F. Garcia-Castro, A. Alberich-Bayarri, and F. Z. Wu, "Identifying pulmonary nodules or masses on chest radiography using deep learning: external validation and strategies to improve clinical practice," Clin Radiol, vol. 75, no. 1, pp. 38–45, Jan. 2020, doi: 10.1016/j.crad.2019.08.005.

[35] S. Bharati, P. Podder, and M. R. H. Mondal, "Hybrid deep learning for detecting lung diseases from X-ray images," Inform Med Unlocked, vol. 20, p. 100391, Jan. 2020, doi: 10.1016/j.imu.2020.100391.

[36] J. Soltani-Nabipour, A. Khorshidi, and B. Noorian, "Lung tumor segmentation using improved region growing algorithm," Nuclear Engineering and Technology, vol. 52, no. 10, pp. 2313–2319, Oct. 2020, doi: 10.1016/j.net.2020.03.011.

[37] M. Horry, S. Chakraborty, B. Pradhan, M. Paul, D. Gomes, and A. Ul-Haq, "Deep Mining Generation of Lung Cancer Malignancy Models from Chest X-ray Images," Sensors (Basel), vol. 21, no. 19, p. 6655, 2021.

[38] J. Lee, S. R. Pant, and H.-S. Lee, "An Adaptive Histogram Equalization Based Local Technique for Contrast Preserving Image Enhancement," The International Journal of Fuzzy Logic and Intelligent Systems, vol. 15, no. 1, pp. 35–44, Mar. 2015, doi: 10.5391/ijfis.2015.15.1.35.

[39] J. Bernsen, "Dynamic thresholding of gray-level images," in Proceedings International Conference on Pattern Recognition, Jan. 1986.

AUTHORS' PROFILE

Dnyaneshwar Kanade Research Scholar, School of Engineering and Technology, Sandip University, Nasik, India. He received the B.E. degree in Electronics Engineering from the Savitribai Phule Pune University (Formerly University of Pune), in 1996 and the M.E degree from Babasaheb Ambedkar Marathwada University, Aurangabad, in 2007. He has 3 Granted Patents on his name. He has published many papers in national and international journals. His research interest includes biomedical signal and image processing, Embedded System Design and IOT. He is a Lifetime member of Indian Society for Technical Education (ISTE).

Dr. Jagdish Helonde Professor, Department of Electrical & Electronics Engineering, School of Engineering and Technology, Sandip University, Nasik, India. He received the B.E. degree in Electrical Engineering from the Govt. College of Engineering, in 1981 and the M.Tech degree from VNIT Nagpur in 1983. He obtained Ph.D. degree in Electrical Engineering from RTM Nagpur University, Nagpur, India in 2002. He has a teaching experience of 40 years. He has guided more than 10 Ph.D scholars. He has published three patents. He has presented 14 papers in National Conferences and 34 in International Conferences. He has published 52 papers in international journals. His research interest includes biomedical signal and image processing, energy management, statistical signal processing, non-conventional energy sources etc. He is a Lifetime member of Institution of Engineers (India) and Indian Society for Technical Education (ISTE).